Received: 28 January 2019 | Revised: 11 March 2019 | Accepted: 18 March 2019

DOI: 10.1002/hbm.24584

WILEY

RESEARCH ARTICLE

Dysfunctional white-matter networks in medicated and unmedicated benign epilepsy with centrotemporal spikes

Yuchao Jiang[1] | Li Song[2] | Xuan Li[1] | Yaodan Zhang[2,3] | Yan Chen[1] | Sisi Jiang[1] | Changyue Hou[2] | Dezhong Yao[1] | Xiaoming Wang[2] | Cheng Luo[1]

[1]The Clinical Hospital of Chengdu Brain Science Institute, MOE Key Lab for Neuroinformation, Center for Information in Medicine, School of Life Science and Technology, University of Electronic Science and Technology of China, Chengdu, People's Republic of China

[2]Neurology Department, Affiliated Hospital of North Sichuan Medical College North Sichuan Medical College, Nanchong, China

[3]Chengdu University of Traditional Chinese Medicine, Chengdu, Sichuan, China

Correspondence
Dezhong Yao and Cheng Luo, The Clinical Hospital of Chengdu Brain Science Institute, MOE Key Lab for Neuroinformation, Center for Information in Medicine, School of Life Science and Technology, University of Electronic Science and Technology of China, Second North Jianshe Road, Chengdu 610054, China.
Email: dyao@uestc.edu.cn; chengluo@uestc.edu.cn

Xiaoming Wang, Neurology Department, Affiliated Hospital of North Sichuan Medical College North Sichuan Medical College, Nanchong 637007, China.
Email: wangxm238@163.com

Funding information
National Nature Science Foundation of China, Grant/Award Numbers: 31771149, 81701778, 81771822, 81861128001; Project of Science and Technology Department of Sichuan Province, Grant/Award Number: 2017JY0179

Abstract

Benign epilepsy with centrotemporal spikes (BECT) is the most common childhood idiopathic focal epilepsy syndrome, which characterized with white-matter abnormalities in the rolandic cortex. Although diffusion tensor imaging research could characterize white-matter structural architecture, it cannot detect neural activity or white-matter functions. Recent studies demonstrated the functional organization of white-matter by using functional magnetic resonance imaging (fMRI), suggesting that it is feasible to investigate white-matter dysfunctions in BECT. Resting-state fMRI data were collected from 24 new-onset drug-naive (unmedicated [NMED]), 21 medicated (MED) BECT patients, and 27 healthy controls (HC). Several white-matter functional networks were obtained using a clustering analysis on voxel-by-voxel correlation profiles. Subsequently, conventional functional connectivity (FC) was calculated in four frequency sub-bands (Slow-5:0.01–0.027, Slow-4:0.027–0.073, Slow-3:0.073–0.198, and Slow-2:0.198–0.25 Hz). We also employed a functional covariance connectivity (FCC) to estimate the covariant relationship between two white-matter networks based on their correlations with multiple gray-matter regions. Compared with HC, the NMED showed increased FC and/or FCC in rolandic network (RN) and precentral/postcentral network, and decreased FC and/or FCC in dorsal frontal network, while these alterations were not observed in the MED group. Moreover, the changes exhibited frequency-specific properties. Specifically, only two alterations were shared in at least two frequency bands. Most of these alterations were observed in the frequency bands of Slow-3 and Slow-4. This study provided further support on the existence of white-matter functional networks which exhibited frequency-specific properties, and extended abnormalities of rolandic area from the perspective of white-matter dysfunction in BECT.

KEYWORDS
benign epilepsy with centrotemporal spikes, epilepsy, fMRI, white-matter functional network

1 | INTRODUCTION

As the most common childhood idiopathic focal epilepsy syndrome, benign epilepsy with centrotemporal spikes (BECT) is characterized with the nocturnal epileptiform spikes arising from the rolandic or

Yuchao Jiang, Li Song, Xuan Li, and Yaodan Zhang contributed equally to this study.

sensorimotor cortex. Although the epileptogenic zone of rolandic spikes originates from the rolandic cortex surrounding the central fissure, it can also lead to disturbances of the cortical and subcortical circuitry (Bouma, Bovenkerk, Westendorp, & Brouwer, 1997; Cao et al., 2017). As the white matter is the structural basis of the conduction of rolandic spikes, it can be hypothesized that the rolandic spikes also damaged the white matter. Recently, Ciumas et al. (2014) demonstrated aberrant white-matter microstructure in the precentral and postcentral gyri using the diffusion tensor imaging (DTI). Cao et al. (2017) indicated reduced white-matter integrity between the corpus callosum and primary sensorimotor cortex in BECT. These neuroimaging studies provided evidence of structural abnormalities in the white matter to support this hypothesis. However, they failed to uncovered dysfunction of the white matter and functional relationship between white-matter networks in BECT.

To date, DTI has been widely used to characterize the structural architecture of the white matter; however, it is unsuitable for the detection of the neural activity and brain functions inside the white matter. Functional magnetic resonance imaging (fMRI) based on blood oxygen level-dependent (BOLD) signals is an effective technique to uncover the neural activity and relevant functions of the gray matter in neuropsychology and clinical neurological diseases (Chen, Liu, et al., 2017; Dong et al., 2018; Duan et al., 2015; Jia et al., 2018; Zhong et al., 2018). Recently, greater attention focused on the detection of neural activation and functional organization in the white matter by using the fMRI (Ding et al., 2018; Fabri & Polonara, 2013; Fabri, Polonara, Mascioli, Salvolini, & Manzoni, 2011; Gawryluk, Mazerolle, Brewer, Beyea, & D'Arcy, 2011; Gawryluk, Mazerolle, & D'Arcy, 2014; Jiang, Luo, Li, Li, et al., 2018; Marussich, Lu, Wen, & Liu, 2017; Peer, Nitzan, Bick, Levin, & Arzyt, 2017). For example, the white-matter functional activation has been observed in multiple tasks including perceptual, language, and motor tasks (Fabri et al., 2011; Fabri & Polonara, 2013; Gawryluk et al., 2011; Gawryluk et al., 2014). Ding et al.'s (2018) studies indicated that the white matter is involved in neural coding and information processing. Marussich et al. (2017) demonstrated that fMRI signals in the white matter contained functional information related to brain activity and connectivity at resting state. Peer et al. (2017) uncovered the intrinsic functional organization in the white matter. These studies provided accumulated evidence for the existence of functional brain activity in the white matter. Furthermore, a recent study found that the functional connectivity (FC) in the white matter is associated with the underlying pathological mechanisms in schizophrenia (Jiang, Luo, Li, Li, et al., 2018) and Parkinson's disease (Ji et al., 2019). These studies suggested that it is feasible to investigate the white-matter dysfunctions in BECT by fMRI.

Although previous research demonstrated the existence of white-matter functional networks and verified their reliability and reproducibility (Ding et al., 2018; Gawryluk et al., 2014; Ji, Liao, Chen, Zhang, & Wang, 2017; Marussich et al., 2017; Peer et al., 2017), it may not be sufficient to fully characterize the white-matter FC. First, the frequency band effect on white-matter FC remained unclear. Previous studies have demonstrated that traditional full frequency band (0–0.25 Hz) could be subdivided into several bands, and distinct frequency bands may reflect differential physiological properties and specific-disorder alterations (Cha, Zatorre, & Schonwiesner, 2016; Duan et al., 2017; Palva & Palva, 2012). Second, the interactions between gray-matter and white-matter networks have not been fully characterized. Because different gray-matter areas are structurally connected by white-matter networks, suggesting that the relationship between gray matter and white matter may be a multilevel network architecture (Jiang, Luo, Li, Li, et al., 2018; Zhang et al., 2011). Thus, except the traditional FC which measures the direct temporal synchronism between two white-matter networks, this study also employed a novel method of functional covariance connectivity (FCC) to estimate the covariant relationship between two white-matter networks based on their correlations with multiple gray-matter regions. We hypothesized that the FCC can capture a complex information interactions white-matter and gray-matter regions. Finally, many neurological disorders including epilepsy, Parkinson's, and Alzheimer's diseases are characterized by white-matter impairments (Bohnen & Albin, 2011; Caso et al., 2015; Xue et al., 2014). Thus, investigation of the white-matter functional networks in brain disorders may contribute to understanding the pathological mechanism and white-matter functions.

In this study, resting-state fMRI data were collected from 24 new-onset drug-naive (unmedicated [NMED]), 21 medicated (MED) BECT patients, and 27 healthy controls (HC). First, based on voxel-by-voxel correlation patterns, an identified clustering analysis was performed within the white matter to obtain several white-matter functional networks. Second, we subdivided the full frequency range into four bands according to previously defined. Subsequently, the traditional FC and FCC were calculated in each frequency band. Finally, by separate comparisons of the white-matter FC among the three groups, we linked the functional disturbances of white matter with the pathological mechanism in BECT.

2 | METHODS

2.1 | Participants

In this study, 24 unmedicated patients with BECT (NMED group, 10 females and 14 males; age: 9.40 ± 2.02 years) were newly diagnosed and did not receive antiepileptic drugs. Twenty-one MED patients with BECT (MED group, 9 females and 12 males; age: 9.64 ± 1.76 years) received monotherapy with valproic acid or levetiracetam. All patients were recruited from the department of the Affiliated Hospital of North Sichuan Medical College (from June 2012 to June 2016). The inclusion criteria included: (a) diagnosis as BECT according to the criteria of the International League Against Epilepsy (Engel and International League Against Epilepsy, 2001) by pediatric epileptologists; (b) without other neurologic psychological disorders; (c) no developmental disabilities; (d) normal routine brain MRI scans. Routine clinical EEG recordings were obtained for all patients. Left-sided spikes were observed in 15 patients (six MED and nine NMED), right-sided spikes were observed in 11 patients (seven MED and four NMED), and bilateral spikes were observed in 19 patients (8 MED and 11 NMED). A sample of 27 healthy subjects (HC group, 10 females and 17 males; age: 10.00 ± 3.74 years) were also included in this

study as a control group. All the healthy subjects confirmed that they had no history of psychiatric and/or neurological disorders. There were no significant differences in the age and gender among the three groups (Table 1). The participant's information were obtained from subjects and her/his parents. The study was reviewed and approved by the Ethics Committee of the Affiliated Hospital of North Sichuan Medical College, and written informed consent was obtained from all the subjects. Then, 21 of the 45 BECT patients have been previously reported in a prior article which examined FC between two intrinsic gray-matter networks of default mode network and task positive network (Luo et al., 2016). And 43 of the 45 BECT patients have been previously reported in a prior article which investigated the asymmetry measured by interhemispheric gray-matter functional connection (Cao et al., 2017). Other than these previous articles, the current study focused on white-matter dysfunctions measured by a novel methodology.

2.2 | Image acquisition

Imaging data were collected using a 3-Tesla MRI scanner (GE DISCOVERY MR750) with an eight-channel standard whole head coil. High-resolution T1-weighted images were obtained by using a three-dimensional fast spoiled gradient-echo sequence. The scanning parameters included: repetition time (TR) = 6.008 ms; echo time (TE) = 1.984 ms; flip angle (FA) = 90°; field of view (FOV) = 25.6 × 25.6 cm^2; matrix size = 256 × 256; and slice thickness = 1 mm (no gap). Resting-state functional data were obtained by using a gradient-echo echo-planar imaging sequence. The main scanning parameters were as follows: TR = 2 s; TE = 30 ms; FA = 90°; FOV = 24 × 24 cm^2; matrix size = 64 × 64; slice thickness = 4 mm (no gap); slice number = 35; and scanning time lasting 410 s (205 volumes). During scanning, participants were instructed to close eyes without falling asleep. After scanning, all the subjects confirmed that they did not fall asleep during scans.

2.3 | Data preprocessing

Similar with our previous study (Jiang, Luo, Li, Li, et al., 2018), the fMRI preprocessing steps included as follows: (a) the first five volumes were discarded, (b) slice-time correction, (c) realignment. Subjects with maximum motion >2 mm or 2° were excluded, (d) linear detrending, (e) regress out the nuisance signal (including 24-parameter motion correction and the mean cerebrospinal fluid [CSF] signals), and (f) temporally scrubbing the motion "spikes." The temporal scrubbing was performed by using a linear regression model with motion "spike" as separate regressor. The motion "spikes" were defined as the time points with a high framewise displacement (FD) > 1. (g) To avoid the mixture of the white-matter and gray-matter signals, spatially smoothing (full width at half maximum (FWHM) = 4 mm) was performed separately within the white-matter or gray-matter masks. In detail, the individual T1 images were segmented into white matter, gray matter, and CSF in native space. The resulting T1 segmentation images were coregistered to the functional space for each participant for the identification of white-matter or gray-matter masks (the threshold was set at 0.5). The individual functional images were smoothed (FWHM = 4 mm) separately within the two masks. (h) Normalization to the standard MNI template. Preprocessing was conducted within the toolkits of the SPM12 (www.fil.ion.ucl.ac.uk/spm) and DPABI (http://rfmri.org/dpabi). As FC is sensitive to head motion, we analyzed the group-level head-motion differences among the three groups using analysis of variance (ANOVA). Seven indices (*x*, *y*, and *z* mean translation and rotation and mean FD) were used to measure the head motion. Results showed no differences of head motion among three groups.

2.4 | Clustering analysis on the fMRI data to obtain the white-matter networks

The clustering strategy refers to our previous study and had three steps (Jiang, Luo, Li, Li, et al., 2018) (Figure 1a).

The first step was to obtain an unified group-level white-matter mask based on high-resolution T1-weighted images. In detail: (a) for each subject, the T1-weighted image was segmented into white matter, gray matter, and CSF, and then normalized to the MNI template. (b) For each voxel, it was identified as white matter, gray matter, or CSF according to its maximum probability from above segmentation results. This generated three masks of white matter, gray matter, and CSF for each subject. (c) We averaged these masks across all the subjects, and thus obtained a percentage of subjects that were classified as white matter or gray matter. A threshold of percentage >60% was used to identify a group-level white-matter mask. (d) The subcortical areas of thalamus, putamen, globus pallidus, caudate, and accumbens from the Harvard–Oxford Atlas

TABLE 1 Demographic and clinical information of subjects

	NMED BECT (*N* = 24)	MED BECT (*N* = 21)	HC (*N* = 27)	*p*-Value
Gender (female/male)	10/14	9/12	10/17	0.922[a]
Age (year)	9.40 ± 2.02	9.64 ± 1.76	10.00 ± 3.74	0.732[b]
Age at onset (year)	8.81 ± 1.88	8.04 ± 2.10	–	0.203[c]
Epilepsy duration (month)	8.33 ± 9.47	21.14 ± 12.01	–	<0.001[c]

Abbreviations: ANOVA, analysis of variance; BECT, benign epilepsy with centrotemporal spikes; HC, healthy control; MED, medicated; NMED, unmedicated.

[a]Chi-square test.

[b]ANOVA.

[c]Two-sample *t* test.

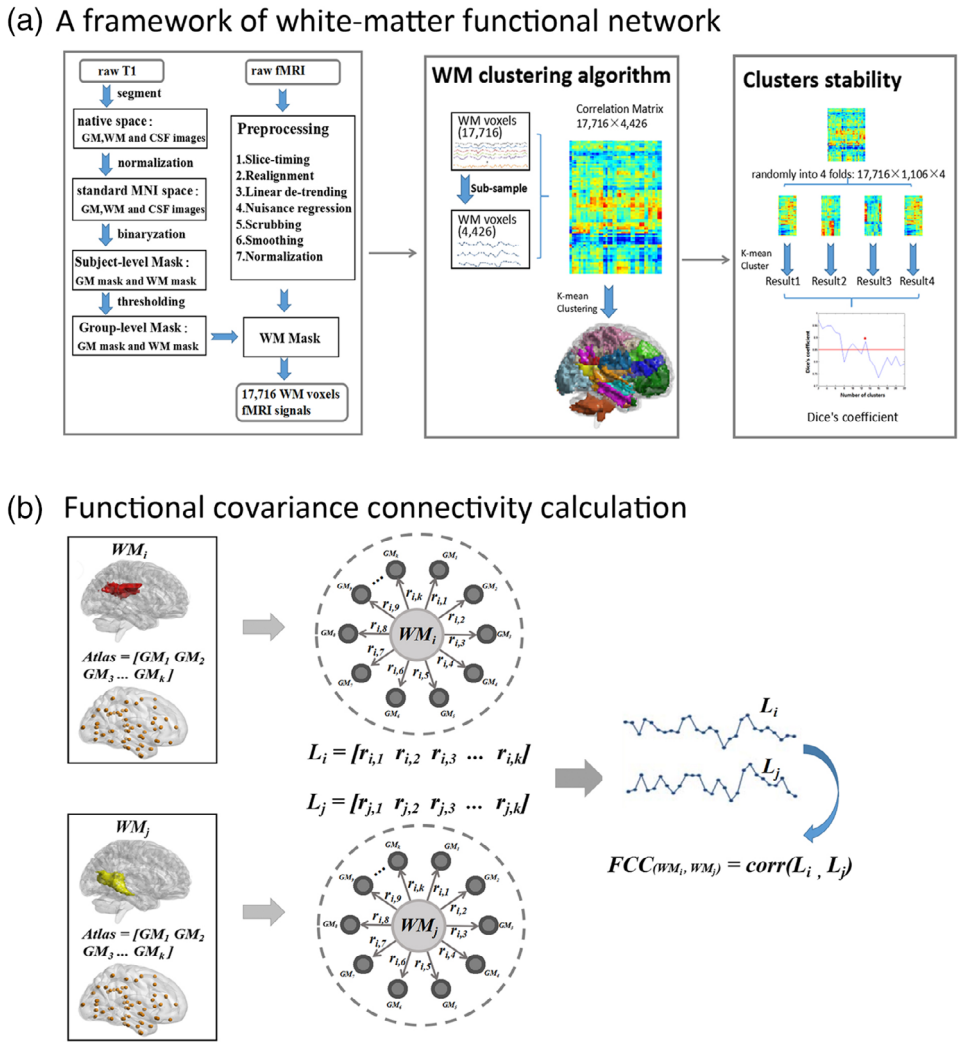

FIGURE 1 Framework of white-matter functional network clustering analysis (a). First, the raw T1 was segmented into gray matter (GM), white matter (WM), and cerebrospinal fluid (CSF), and then normalized to the MNI space. The subject-level GM, WM masks were obtained based on maximum probability of each voxel and subsequently averaged to identify a group-level WM mask. Second, raw fMRI were preprocessed, and time series of 17,716 voxels were extracted from WM mask. Third, 17,716 voxels were subsampled to 4,426 nodes to reduce computational complexity. Pearson's correlation coefficient between each voxel and each node was calculated, and this resulted in a 17,716 × 4,426 correlation matrix for each subject. A K-means clustering analysis (distance metric correlation, 10 replicates) was performed on the averaged correlation matrix across all subjects. Finally, we randomly divided the averaged connectivity matrix (17,716 × 4,426) into four folds (17,716 × 1,106). The same clustering computation was performed on each fold separately. This resulted in four clustering results. By measuring the similarity of the clustering results between any two folds using Dice's coefficient, the stability of clusters were evaluated. (b) Calculation of functional covariance connectivity (FCC). Based on the idea of "correlation of correlations," FCC was used to estimate the covariant relationship between two WM networks based on their correlations with multiple GM regions [Color figure can be viewed at wileyonlinelibrary.com]

(threshold = 25%) were removed from the group-level white-matter mask to further correct the deep brain structures (Lorio et al., 2016; Peer et al., 2017; Wonderlick et al., 2009). (e) Finally, the group-level white-matter mask was coregistered to the functional space and resampled a same voxel size with fMRI images. This white-matter mask consisted of 17,716 voxels. In addition, a gray-matter mask was also obtained using the same procedures. There was no overlapped area between white-matter mask and gray-matter mask.

The second step applied the K-means clustering algorithm to obtain white-matter spatial networks. (a) To reduce the computational complexity, the 17,716 voxels within the white matter were subsampled to 4,426 nodes based on an interchanging grid strategy (Craddock, James, Holtzheimer, Hu, & Mayberg, 2012). (b) For each subject, the Pearson's correlation coefficient between each voxel and each node was calculated, and this resulted in an 17,716 × 4,426 correlation matrix. (c) These correlation matrices were averaged across all the subjects. (d) A K-means clustering analysis (distance metric correlation, 10 replicates) was performed on the averaged correlation matrix. This step clustered all the white-matter voxels into K-independent spatial networks.

The third step is used to evaluate the stability of the K (the number of clusters). (a) We randomly divided the averaged connectivity

matrix (17,716 × 4,426) into four folds (17,716 × 1,106). (b) The same clustering computation was performed on each fold separately. This resulted in four clustering results. (c) To measure the similarity of the clustering results between any two folds, an adjacency matrix was calculated for each clustering result from each fold, and these adjacency matrices were then compared using Dice's coefficient. The averaged Dice's coefficient was used to evaluate the stability of clusters. (d) Multiple K (the numbers of clusters ranged from 2 to 22) was considered in this study. For each K, the clustering computation was performed separately and obtained a Dice's coefficient to reflect its stability.

2.5 | Decomposing the BOLD time series in different frequency bands

Previous studies have shown that the low frequency range could be subdivided into several bands and specific frequency bands may carry specific properties or physiological functions (Cha et al., 2016; Duan et al., 2017; Palva & Palva, 2012). Here, we subdivided the low frequency range into four bands according to previously defined (Buzsaki & Draguhn, 2004; Zuo et al., 2010): Slow-5 (0.01–0.027 Hz), Slow-4 (0.027–0.073 Hz), Slow-3 (0.073–0.198 Hz), and Slow-2 (0.198–0.25 Hz). In addition, we also examined the full frequency range (0–0.25 Hz).

2.6 | FC of white-matter networks

Conventional FC was used to measure the relationship between two white-matter networks. For each subject, the Pearson's correlation coefficient between the average time courses of any two white-matter networks was computed and transformed to the Fisher *z* score.

In addition, we employed an FCC method, which is based on the idea of "correlation of correlations," to estimate the covariant relationship between two white-matter networks based on their correlations with multiple gray-matter regions. First, gray-matter regions (n = 96) were defined according to the Harvard–Oxford gray-matter atlas (Desikan et al., 2006). The gray-matter mask was used as a restriction for gray-matter voxels. Only the time series within the intersection between gray-matter mask and Harvard–Oxford atlas were extracted. Second, the Pearson's correlations were calculated between each white-matter network and each gray-matter region, and this obtained a K × 96 correlation matrix (K is the number of white-matter networks). Third, the FCC was estimated between any two white-matter networks, and this generated a K × K FCC matrix. The FCC_{ij} is defined as follows:

$$FCC_{ij} = \mathrm{corr}(FC_i, FC_j)$$

where FC_i represents the vector of FC values between the white-matter network i and all 96 gray-matter regions; FC_j is the vector of FC values between the white-matter network j and all 96 gray-matter regions; and FCC_{ij} is the Pearson's correlation between FC_i and FC_j. The FCC value was further transformed to the Fisher *z* score. A flowchart of FCC calculation is shown in Figure 1b.

In addition, the differences between FCC and FC may be several points. First, a fundamental difference may come from its definition. Since FCC is the correlation of FC profiles, it may magnify the subtle differences, and contribute to the distinction between healthy and diseases (Zhao, Zhang, Rekik, An, & Shen, 2018). Second, the FC is the correlation between BOLD signals of two regions, so it could only reflect information from two limited regions (i.e., one-to-one information flow). In contrast, by integrating the information from many regions, the FCC carries complex information interaction (i.e., one-to-many-to-one information flow). Third, since FCC is calculated indirectly rather than directly using BOLD time series, FCC may be not easily altered by noise and artifacts (Zhang et al., 2016). Because in FCC calculation, this noise contaminated FC may be only one element of the FC profiles. In spite of these advantages of FCC, we also recognized that FC is one of the most useful methods for fMRI studies. We considered that FCC and FC are complementary and contributed to the interpretation in fMRI studies. In this study, for each subject and each frequency band, both FC and FCC were calculated and used for the following statistical analysis.

2.7 | Statistical analysis

One-sample *t* tests were first performed to determine the significant FC and FCC for each group and each frequency band. The Bonferroni correction was used for the multiple comparisons correction. Subsequently, for these significant FC and FCC, ANOVA and post hoc analysis were used to compare the differences among the NMED, MED, and HC groups, with the Sidak correction for the multiple comparisons correction (Abdi, 2007).

3 | RESULTS

3.1 | White-matter functional networks

In this study, we evaluated the stability of the number of white-matter networks by the Dice's coefficient. The results showed that the K = 13 is the largest number with a high stability (Dice's coefficient >0.85) (Figure 2); thus, 13 white-matter networks were used in subsequent analysis. According to the spatial location of network, these networks could be named as: WM1 (ventral frontal network), WM2 (posterior temporal network), WM3 (corona radiate network), WM4 (dorsal frontal network), WM5 (occipital network), WM6 (anterior temporal network), WM7 (orbitofrontal network), WM8 (inferior longitudinal fasciculus network), WM9 (temporoparietal network), WM10 (cerebellar network), WM11 (posterior corpus callosum network), WM12 (RN), and WM13 (precentral/postcentral network, PCN) (Figure 2 and Table 2). Interestingly, the WM12 located at the bilateral superficial white-matter area under the rolandic cortex.

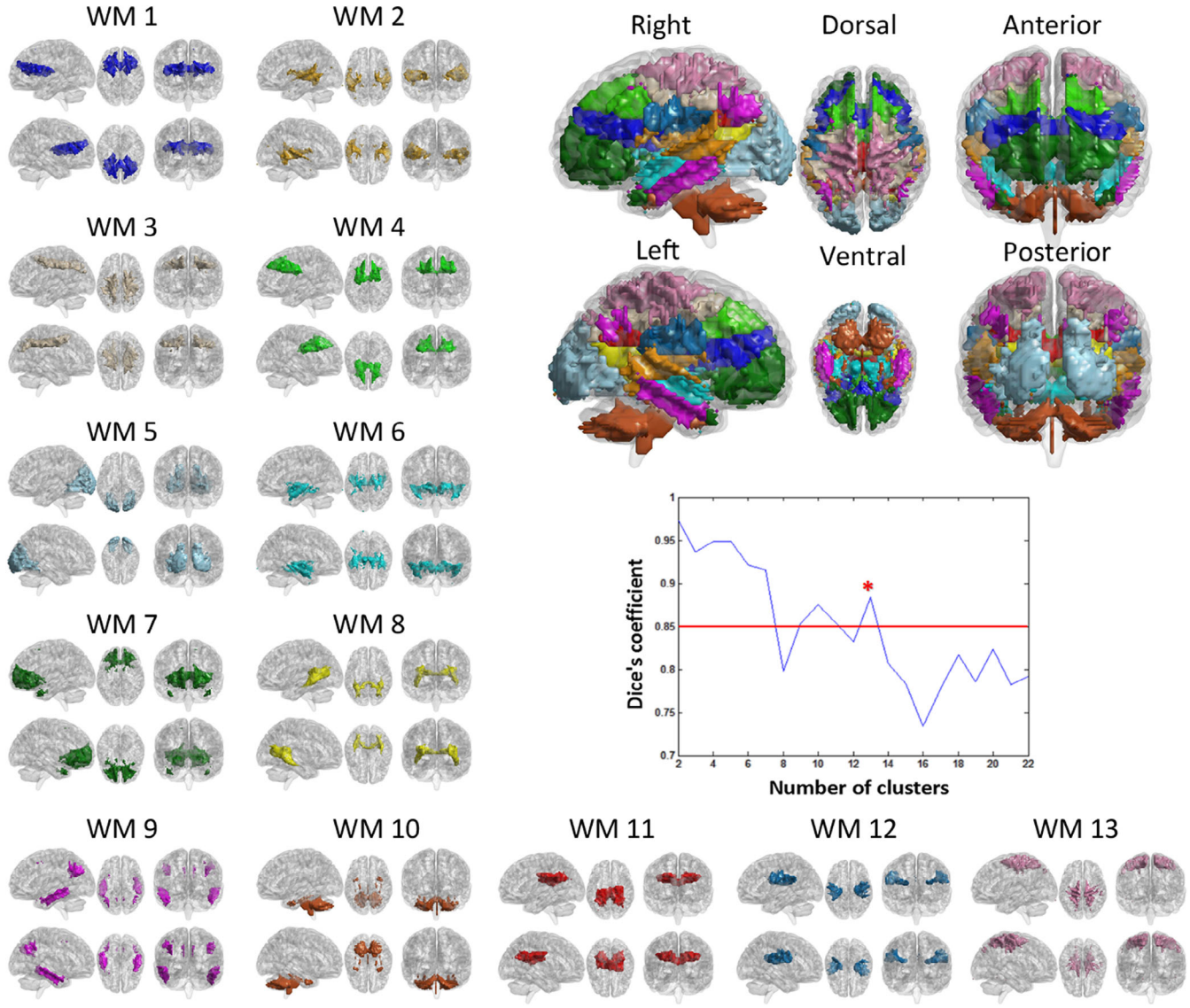

FIGURE 2 White-matter (WM) functional networks and stability of clustering for different numbers of clusters, measured by Dice's coefficient. WM1 (ventral frontal network, VFN), WM2 (posterior temporal network, PTN), WM3 (corona radiate network, CRN), WM4 (dorsal frontal network, DFN), WM5 (occipital network, ON), WM6 (anterior temporal network, ATN), WM7 (orbitofrontal network, OFN), WM8 (inferior longitudinal fasciculus network, ILFN), WM9 (temporoparietal network, TPN), WM10 (cerebellar network, CN), WM11 (posterior corpus callosum network, PCCN), WM12 (Rolandic network, RN), and WM13 (precentral/postcentral network, PCN) [Color figure can be viewed at wileyonlinelibrary.com]

3.2 | Differences of FC in each frequency band among NMED, MED, and HC

In the full frequency band, two FCs (WM2–WM12 [F = 6.34, p = 0.0029] and WM4–WM12 [F = 5.09, p = 0.0086]) showed significant group effects among the NMED, MED, and HC groups by the ANOVA (Figure 3a). The post hoc analyses further revealed that the NMED had a higher FC of the WM2–WM12 than the MED and the HC group (Figure 3a′). In addition, the NMED exhibited a reduced FC in the WM4–WM12 than the MED group (Figure 3a′).

In the band Slow-2, no significant group effect was observed by the ANOVA (Figure 3b).

In the band Slow-3, the ANOVA found two FCs (WM2–WM12 [F = 5.66, p = 0.0053] and WM10–WM12 [F = 7.76, p = 0.00091]) with significant differences among the three groups (Figure 3c). In detail, an increased FC of WM2–WM12 was observed in the NMED group compared with the other two groups (Figure 3c′). Additionally, the MED group showed a decreased FC of the WM10–WM12 than both groups of the NMED and the HC (Figure 3c′).

In the band Slow-4, significant group effects were observed in the three FCs of the WM2–WM12 (F = 5.50, p = 0.0061), WM3–WM13 (F = 6.20, p = 0.0033), and WM4–WM12 (F = 5.64, p = 0.0054) (Figure 3d). The NMED exhibited a higher FC in the WM2–WM12 than the other two groups and a higher FC of the WM3–WM13 than

TABLE 2 White-matter functional networks

Number	White-matter network	Abbreviation
WM1	Ventral frontal network	VFN
WM2	Posterior temporal network	PTN
WM3	Corona radiate network	CRN
WM4	Dorsal frontal network	DFN
WM5	Occipital network	ON
WM6	Anterior temporal network	ATN
WM7	Orbitofrontal network	OFN
WM8	Inferior longitudinal fasciculus network	ILFN
WM9	Temporoparietal network	TPN
WM10	Cerebellar network	CN
WM11	Posterior corpus callosum network	PCCN
WM12	Rolandic network	RN
WM13	Precentral/postcentral network	PCN

the HC (Figure 3d′). In addition, compared with the NMED and the HC, the MED showed an enhanced FC in the WM4–WM12 (Figure 3d′).

Finally, in the band Slow-5, only one FC (WM3–WM4 [F = 5.02, p = 0.0092]) showed a significant group difference (Figure 3e). Compared with the HC, both the NMED and the MED groups showed reduced FC (Figure 3e′).

3.3 | Differences of FCC in each frequency band among NMED, MED, and HC

In the full frequency band, the ANOVA indicated the significant group effects in the three FCCs of the WM2–WM12 [F = 6.35, p = 0.0029]; WM3–WM4 [F = 5.51, p = 0.0060]; and WM8–WM13 [F = 6.26, p = 0.0032] (Figure 4a). Specifically, post hoc analyses showed that the NMED had an increased FCC of the WM2–WM12 than the other two groups (Figure 4a′). In addition, compared with the HC group, the NMED group exhibited a reduced FCC in the WM3–WM4 and an enhanced FCC in the WM8–WM13 (Figure 4a′).

In the band Slow-2, only one FCC (WM4–WM7 [F = 5.05, p = 0.0089]) showed significant difference among the three groups (Figure 4b). The post hoc analysis manifests that the NMED had a higher FCC than both groups of the MED and the HC (Figure 4b′).

In the band Slow-3, there were four FCCs (WM2–WM12 [F = 6.41, p = 0.0028]; WM2–WM13 [F = 5.64, p = 0.0053]; WM3–WM4 [F = 5.82, p = 0.0046]; and WM4–WM12 [F = 6.72, p = 0.0021]) with significant group effects by the ANOVA (Figure 4c). In detail, compared with the MED and the HC, the NMED exhibited increased FCCs in the WM2–WM12 and the WM2–WM13 and a decreased FCC in the WM4–WM12 (Figure 4c′). Additionally, the NMED showed a reduced FCC of the WM3–WM4 than the HC group (Figure 4c′).

In the band Slow-4, three FCCs (WM2–WM12 [F = 4.94, p = 0.0099]; WM3–WM13 [F = 6.39, p = 0.0028]; and WM8–WM13 [F = 6.21, p = 0.0031]) showed significant group differences (Figure 4d). The post hoc analyses further indicated that the NMED had a higher FCC of the WM2–WM12 than the MED and increased FCCs in the WM3–WM13 and the WM8–WM13 than the HC (Figure 4d′).

Finally, in the band Slow-5, only one FCC of the WM3–WM4 (F = 5.45, p = 0.0063) showed a significant group effect (Figure 4e). The NMED exhibited a reduced FCC than the HC (Figure 4e′).

4 | DISCUSSION

Consistent with previous studies (Jiang, Luo, Li, Li, et al., 2018; Peer et al., 2017), we obtained spatially independent functional networks within white matter by using an identified clustering analysis on resting-state fMRI data. By the evaluation of the FC and FCC in different frequency bands and the comparisons among the NMED, MED, and HC groups, we found that: () compared with the HC, the NMED showed increased FC and/or FCC in the white-matter RN and PCN, and decreased FC and/or FCC in the white-matter dorsal frontal network, which normalized in the MED group. (b) These alterations exhibited frequency-specific properties. Specifically, only two alterations (WM2–WM12 and WM3–WM4) were shared in at least two frequency bands. Most of these alterations were observed in the frequency bands of Slow-3 and Slow-4. (c) Consistent findings of differences in WM2–WM12, WM3–WM13, WM3–WM4, and WM4–WM12 were detected by using the FC and FCC. However, the utilization of FCC excavated additional changes in the WM8–WM13, WM4–WM7, and WM2–WM13. In general, these findings provided further support on the existence of white-matter functional networks, and extended the understanding of white-matter impairments and pathological mechanism in BECT.

Previous studies provided both structural and functional evidences of the abnormalities in the rolandic and sensorimotor areas in BECT. For example, larger cortical gray matter volumes of sensorimotor cortices were observed in children with BECT compared to HC (Kim et al., 2015; Luo et al., 2015). DTI studies found reduced fractional anisotropy in the bilateral primary sensorimotor regions (Cao et al., 2017; Ciumas et al., 2014). Resting-state fMRI studies also reported reduced FC in the Rolandic areas (Luo et al., 2015). Ji, Yu et al. (2017) found decreased connectivity strength and regional efficiency in the peri-Rolandic areas by applying graph theoretical analysis on fMRI. Recently, Li et al. (2017) reported decreased functional variability in the sensorimotor-related circuitry by a dynamic FC analysis. The current study supported and extended previous findings of the abnormalities in the rolandic from the perspective of the white-matter dysfunction. The enhanced FC in the white matter may suggest an excessive information transmission within the white matter and may be a possible basis that explains the deficits of the rolandic cortex in BECT. In addition, we observed a reduced FC in the white-matter dorsal frontal network, which may be responsible for the cognitive impairments emerged in BECT patients (Adebimpe, Bourel-Ponchel, & Wallois, 2018).

Although previous studies have provided valuable findings on brain abnormalities in children with BECT, most of these studies recruited chronic and MED patients with BECT, which may introduce

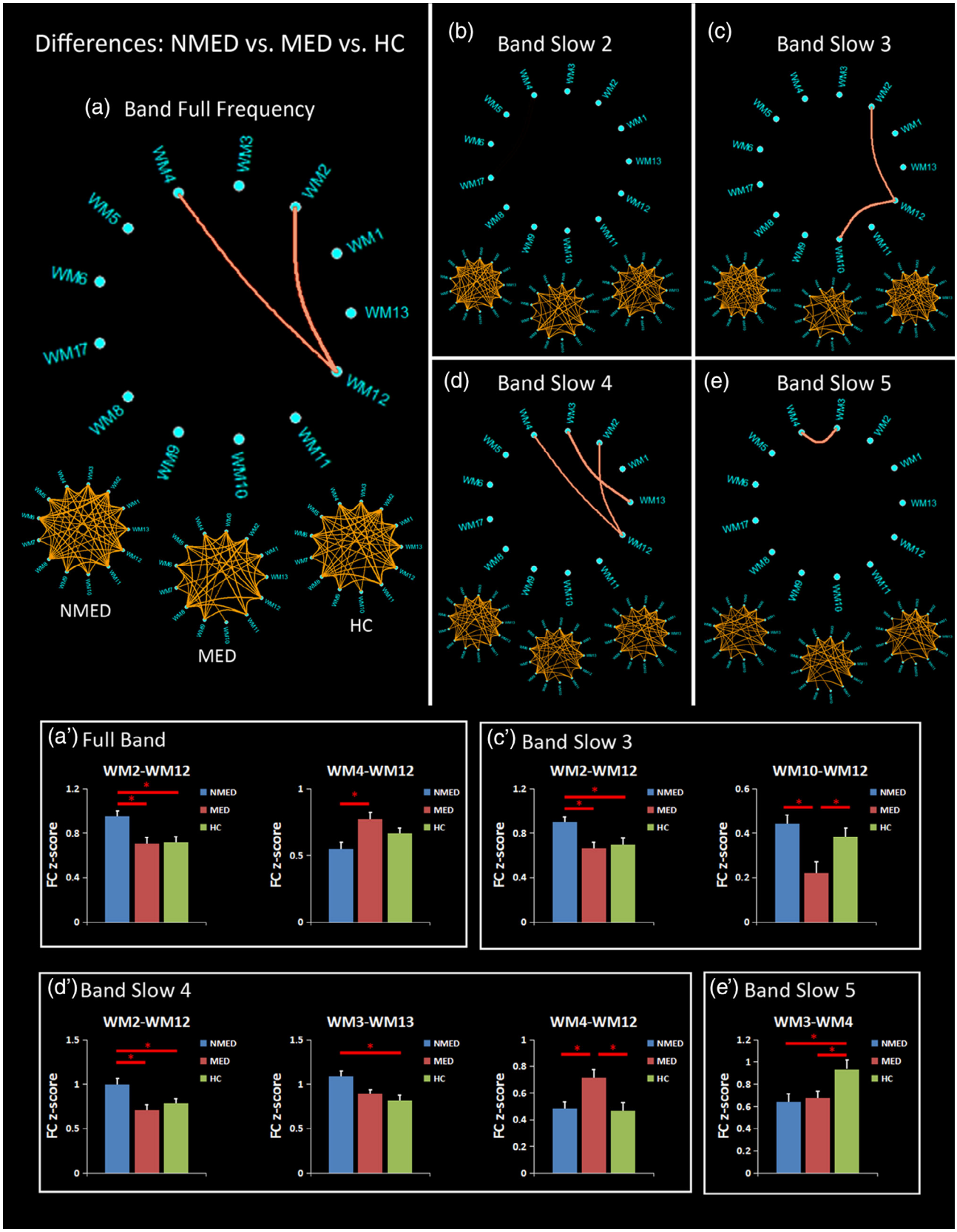

FIGURE 3 Differences of functional connectivity (FC) among the unmedicated benign epilepsy with centrotemporal spikes (NMED BECT), medicated BECT (MED) and healthy controls (HC), measured by analysis of variance (ANOVA) and post hoc analyses for the (a) full frequency band: 0–0.25 Hz, and four frequency sub-bands of (b) Slow-2:0.198–0.25 Hz; (c) Slow-3:0.073–0.198 Hz; (d) Slow-4:0.027–0.073 Hz; and (e) Slow-5:0.01–0.027 Hz. The three under circular graph represents the significant FC in the NMED BECT, MED BECT, and HC, measured by one-sample *t* test. The upper circular graph represents the differences of FC among the NMED, MED, and HC groups, measured by ANOVA. The post hoc analyses are shown in the (a′–e′) [Color figure can be viewed at wileyonlinelibrary.com]

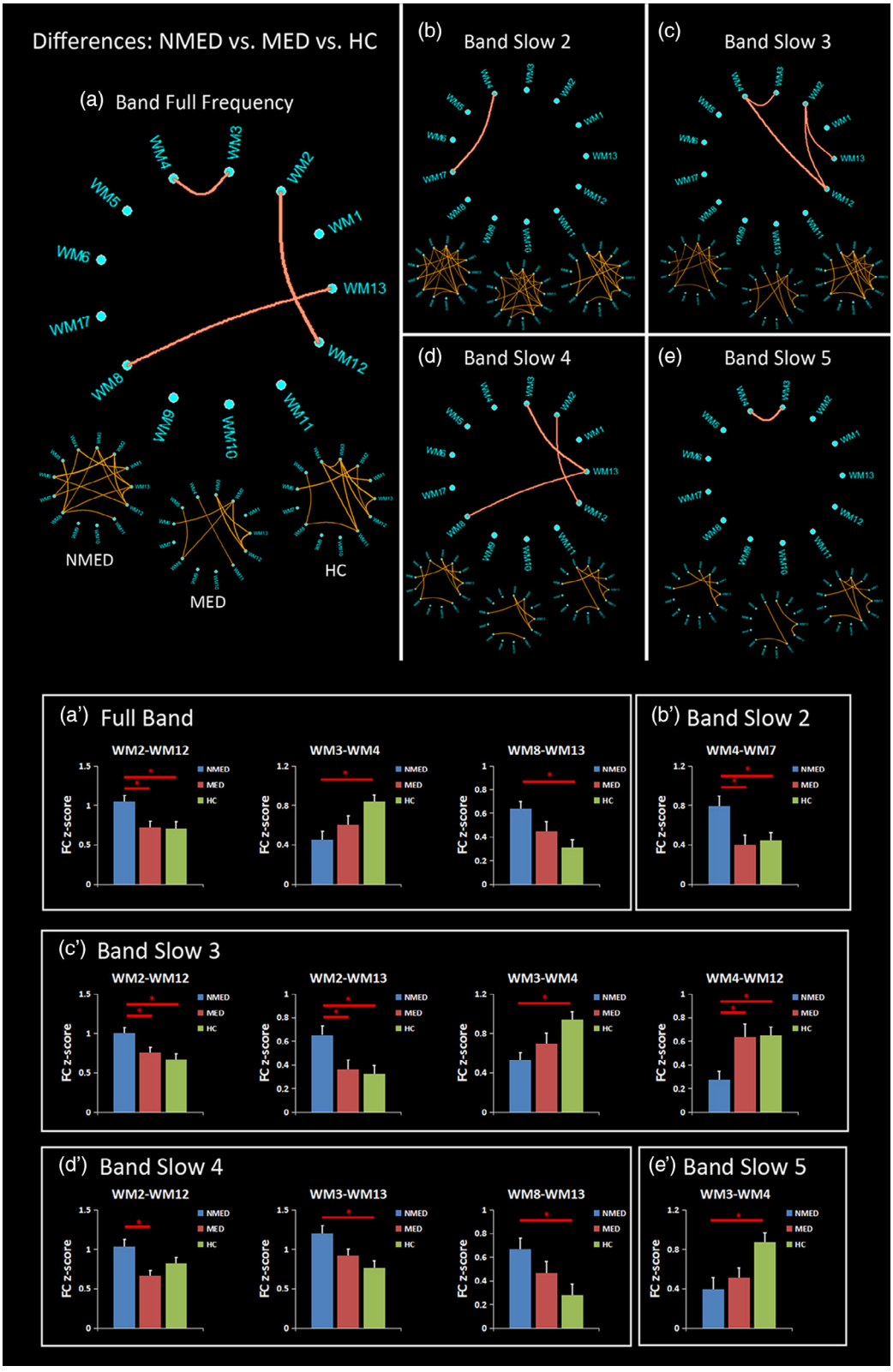

FIGURE 4 Differences of functional covariance connectivity (FCC) among the unmedicated benign epilepsy with centrotemporal spikes (NMED BECT), medicated BECT (MED), and healthy controls (HC), measured by analysis of variance (ANOVA) and post hoc analyses in the (a) full frequency band: 0–0.25 Hz, and four frequency sub-bands of (b) Slow-2:0.198–0.25 Hz; (c) Slow-3:0.073–0.198 Hz; (d) Slow-4:0.027–0.073 Hz; and (e) Slow-5:0.01–0.027 Hz. The three under circular graph represents the significant FC in the NMED BECT, MED BECT, and HC, measured by one-sample *t* test. The upper circular graph represents the differences of FC among the NMED, MED, and HC groups, measured by ANOVA. The post hoc analyses are shown in the (a′–e′) [Color figure can be viewed at wileyonlinelibrary.com]

confounding factors of antiepileptic treatment or long illness duration. Previous studies have demonstrated cumulative medication exposure could significantly affect brain activation and connectivity in both anatomical and functional neuroimaging studies (Datta et al., 2013; Yang et al., 2012; Yang et al., 2013; Zeng et al., 2015). Hence, investigation on the new-onset drug-naive NMED patients and MED patients can provide naive information to the neurobiology of BECT and can also evaluate the effect of anti-epilepsy drugs. Similar with a previous study investigating the local regional homogeneity changes in new-onset versus chronic BECT (Zeng et al., 2015), the current study found that most changes in the new-onset drug-naive NMED BECT patients were normalized in the MED group, suggesting that antiepileptic medication may reverse this aberrant connectivity and even reach a normalized level when compared with healthy subjects. However, these interpretations from cross-sectional findings required further confirmation in future longitudinal research.

Frequency-specific functional alterations within gray matter have been widely observed in cognitive processes and brain diseases (Martino et al., 2016; Wang et al., 2017; Yu et al., 2014). In the current study, the frequency effect of the white-matter dysfunction associated with BECT could be understood from three points. First, the frequency sub-bands contained all of the BECT alterations in the full frequency band but characterized more differences (Jiang, Luo, Li, Li, et al., 2018). This suggested that the application of frequency division could excavate more disease-related functional information within white matter. Second, most of alterations were not shared across sub-bands, which implied a frequency-dependent dysfunction connectivity of brain white matter in each sub-band (Wang et al., 2018). Third, more differences were observed in the frequency band of Slow-3 and Slow-4, suggesting a correspondence between specific frequency and certain disease (Zhao, Tang et al., 2018; Zhou, Huang, Zhuang, Gao, & Gong, 2017). These inferences still need to be verified in future studies to elucidate frequency-specific network organization mechanism. Overall, these frequency-specific findings were consistent with recent perspective of brain networks had distinctive intrinsic frequency (Gohel & Biswal, 2015; Siegel, Donner, & Engel, 2012), which provide a new perspective to decoding complicated brain network from the way of frequency.

While considerable research has used temporal coupling of BOLD signals (i.e., FC) to reveal information exchange among brain areas (Jiang et al., 2017; Jiang, Luo, Gong, Peng, et al., 2018; Zhu et al., 2018), rich high-order information interactions such as dynamic (He et al., 2018; Hutchison et al., 2013; Klugah-Brown et al., 2018), causal (Chen, Jiang, et al., 2017; Jiang, Luo, Li, Duan, et al., 2018), hierarchical (Smith et al., 2013), and many-to-many (Pessoa, 2014) have not been fully explored yet. To characterize a complex relationship between white-matter and gray-matter regions, this study measured the functional resemblance between any two white-matter networks based on their connectivity profiles with gray-matter regions. Using the straightforward approach, we further found new disease-related alterations such as WM2–WM13, WM8–WM13, and WM4–WM7. Since FCC focuses on the topographical FC patterns rather than original BOLD temporal correlations, potential information could be revealed (Zhang et al., 2016). This result suggested that the similarity of the topographical FC profiles may provide effective detection of additional biomarkers in clinical neuroscience applications.

Several limitations should be considered when interpreted these findings. First, although it remains unknown about what functional organization in the white matter represents in terms of physiological signification (Gawryluk et al., 2014), these findings from white matter may add an additional route to uncover the brain mechanism in health and diseases. Second, since the foundations of white-matter fMRI are unclear, some methodological issues such as head motion, respiration, and other artifacts should be further addressed in future work. Third, another shortage of this study includes the relative small sample size and the difference of the illness duration between two patient groups. A larger sample is needed to verify the reliability and reproducibility in the future. Fourth, additional neuropsychological tests are needed to evaluate the association between the white-matter alterations and cognitive impairments.

5 | CONCLUSION

This study extended abnormalities of rolandic area from the perspective of white-matter dysfunction in BECT. The increased white-matter FC may suggest an excessive information exchange under the rolandic area and the reduced FC in frontal area may be responsible for the cognitive impairments. Furthermore, most changes in the new-onset drug-naive NMED BECT patients were normalized in the MED group, suggesting that antiepileptic medication could reverse aberrant connectivity and even reach a normalized level. In addition, disease-related white-matter FCs exhibited frequency-specific properties, which suggests a correspondence between specific frequency and certain disease. Finally, a straightforward metric by measuring the similarity of the topographical FC profiles could provide more effective detection of additional brain dysfunctions in BECT. In general, these findings provided further support on the existence of white-matter functional networks, and extended the understanding of white-matter impairments and pathological mechanism in abnormal brain.

CONFLICT OF INTEREST

The authors declare no potential conflict of interest.

REFERENCES

Abdi, H. (2007). Bonferroni and Šidák corrections for multiple comparisons. *Encyclopedia of Measurement and Statistics*, *3*, 103–107.

Adebimpe, A., Bourel-Ponchel, E., & Wallois, F. (2018). Identifying neural drivers of benign childhood epilepsy with centrotemporal spikes. *Neuroimage Clinical*, *17*, 739–750.

Bohnen, N. I., & Albin, R. L. (2011). White matter lesions in Parkinson disease. *Nature Reviews. Neurology*, *7*, 229–236.

Bouma, P. A., Bovenkerk, A. C., Westendorp, R. G., & Brouwer, O. F. (1997). The course of benign partial epilepsy of childhood with centrotemporal spikes: A meta-analysis. *Neurology*, *48*, 430–437.

Buzsaki, G., & Draguhn, A. (2004). Neuronal oscillations in cortical networks. *Science*, *304*, 1926–1929.

Cao, W., Zhang, Y., Hou, C., Yang, F., Gong, J., Jiang, S., … Yao, D. (2017). Abnormal asymmetry in benign epilepsy with unilateral and bilateral centrotemporal spikes: A combined fMRI and DTI study. *Epilepsy Research*, *135*, 56–63.

Caso, F., Agosta, F., Mattavelli, D., Migliaccio, R., Canu, E., Magnani, G., … Filippi, M. (2015). White matter degeneration in atypical Alzheimer disease. *Radiology*, *277*, 162–172.

Cha, K., Zatorre, R. J., & Schonwiesner, M. (2016). Frequency selectivity of voxel-by-voxel functional connectivity in human auditory cortex. *Cerebral Cortex*, *26*, 211–224.

Chen, X., Jiang, Y., Chen, L., He, H., Dong, L., Hou, C., … Luo, C. (2017). Altered hippocampo-cerebello-cortical circuit in schizophrenia by a spatiotemporal consistency and causal connectivity analysis. *Frontiers in Neuroscience*, *11*, 25.

Chen, X., Liu, C., He, H., Chang, X., Jiang, Y., Li, Y., … Yao, D. (2017). Transdiagnostic differences in the resting-state functional connectivity of the prefrontal cortex in depression and schizophrenia. *Journal of Affective Disorders*, *217*, 118–124.

Ciumas, C., Saignavongs, M., Ilski, F., Herbillon, V., Laurent, A., Lothe, A., … Ryvlin, P. (2014). White matter development in children with benign childhood epilepsy with centro-temporal spikes. *Brain : A Journal of Neurology*, *137*, 1095–1106.

Craddock, R. C., James, G. A., Holtzheimer, P. E., Hu, X. P. P., & Mayberg, H. S. (2012). A whole brain fMRI atlas generated via spatially constrained spectral clustering. *Human Brain Mapping*, *33*, 1914–1928.

Datta, A. N., Oser, N., Bauder, F., Maier, O., Martin, F., Ramelli, G. P., … Penner, I. K. (2013). Cognitive impairment and cortical reorganization in children with benign epilepsy with centrotemporal spikes. *Epilepsia*, *54*, 487–494.

Desikan, R. S., Segonne, F., Fischl, B., Quinn, B. T., Dickerson, B. C., Blacker, D., … Killiany, R. J. (2006). An automated labeling system for subdividing the human cerebral cortex on MRI scans into gyral based regions of interest. *NeuroImage*, *31*, 968–980.

Ding, Z. H., Huang, Y. L., Bailey, S. K., Gao, Y. R., Cutting, L. E., Rogers, B. P., … Gore, J. C. (2018). Detection of synchronous brain activity in white matter tracts at rest and under functional loading. *Proceedings of the National Academy of Sciences of the United States of America*, *115*, 595–600.

Dong, D., Duan, M., Wang, Y., Zhang, X., Jia, X., Li, Y., … Luo, C. (2018). Reconfiguration of dynamic functional connectivity in sensory and perceptual system in schizophrenia. *Cerebral Cortex*. https://doi.org/10.1093/cercor/bhy232

Duan, M., Chen, X., He, H., Jiang, Y., Jiang, S., Xie, Q., … Yao, D. (2015). Altered basal ganglia network integration in schizophrenia. *Frontiers in Human Neuroscience*, *9*, 561.

Duan, X., Chen, H., He, C., Long, Z., Guo, X., Zhou, Y., … Chen, H. (2017). Resting-state functional under-connectivity within and between large-scale cortical networks across three low-frequency bands in adolescents with autism. *Progress in Neuro-Psychopharmacology & Biological Psychiatry*, *79*, 434–441.

Engel, J., Jr., & International League Against Epilepsy. (2001). A proposed diagnostic scheme for people with epileptic seizures and with epilepsy: Report of the ILAE task force on classification and terminology. *Epilepsia*, *42*, 796–803.

Fabri, M., & Polonara, G. (2013). Functional topography of human corpus callosum: An FMRI mapping study. *Neural Plasticity*, *2013*, 251308.

Fabri, M., Polonara, G., Mascioli, G., Salvolini, U., & Manzoni, T. (2011). Topographical organization of human corpus callosum: An fMRI mapping study. *Brain Research*, *1370*, 99–111.

Gawryluk, J. R., Mazerolle, E. L., Brewer, K. D., Beyea, S. D., & D'Arcy, R. C. (2011). Investigation of fMRI activation in the internal capsule. *BMC Neuroscience*, *12*, 56.

Gawryluk, J. R., Mazerolle, E. L., & D'Arcy, R. C. (2014). Does functional MRI detect activation in white matter? A review of emerging evidence, issues, and future directions. *Frontiers in Neuroscience*, *8*, 239.

Gohel, S. R., & Biswal, B. B. (2015). Functional integration between brain regions at rest occurs in multiple-frequency bands. *Brain Connectivity*, *5*, 23–34.

He, H., Luo, C., Luo, Y., Duan, M., Yi, Q., Biswal, B. B., & Yao, D. (2018). Reduction in gray matter of cerebellum in schizophrenia and its influence on static and dynamic connectivity. *Human Brain Mapping*, *40*, 517–528.

Hutchison, R. M., Womelsdorf, T., Allen, E. A., Bandettini, P. A., Calhoun, V. D., Corbetta, M., … Chang, C. (2013). Dynamic functional connectivity: Promise, issues, and interpretations. *NeuroImage*, *80*, 360–378.

Ji, G. J., Liao, W., Chen, F. F., Zhang, L., & Wang, K. (2017). Low-frequency blood oxygen level-dependent fluctuations in the brain white matter: More than just noise. *Scientific Bulletin*, *62*, 656–657.

Ji, G. J., Ren, C., Li, Y., Sun, J., Liu, T., Gao, Y., … Wang, K. (2019). Regional and network properties of white matter function in Parkinson's disease. *Human Brain Mapping*, *40*, 1253–1263.

Ji, G. J., Yu, Y., Miao, H. H., Wang, Z. J., Tang, Y. L., & Liao, W. (2017). Decreased network efficiency in benign epilepsy with centrotemporal spikes. *Radiology*, *283*, 186–194.

Jia, X., Ma, S., Jiang, S., Sun, H., Dong, D., Chang, X., … Luo, C. (2018). Disrupted coupling between the spontaneous fluctuation and functional connectivity in idiopathic generalized epilepsy. *Frontiers in Neurology*, *9*, 838.

Jiang, S., Luo, C., Gong, J., Peng, R., Ma, S., Tan, S., … Yao, D. (2018). Aberrant thalamocortical connectivity in juvenile myoclonic epilepsy. *International Journal of Neural Systems*, *28*, 1750034.

Jiang, Y., Duan, M., Chen, X., Chang, X., He, H., Li, Y., … Yao, D. (2017). Common and distinct dysfunctional patterns contribute to triple network model in schizophrenia and depression: A preliminary study. *Progress in Neuro-Psychopharmacology & Biological Psychiatry*, *79*, 302–310.

Jiang, Y., Luo, C., Li, X., Duan, M., He, H., Chen, X., … Yao, D. (2018). Progressive reduction in gray matter in patients with schizophrenia assessed with MR imaging by using causal network analysis. *Radiology*, *287*, 633–642.

Jiang, Y., Luo, C., Li, X., Li, Y., Yang, H., Li, J., … Yao, D. (2018). White-matter functional networks changes in patients with schizophrenia. *NeuroImage*. https://doi.org/10.1016/j.neuroimage.2018.04.018

Kim, E. H., Yum, M. S., Shim, W. H., Yoon, H. K., Lee, Y. J., & Ko, T. S. (2015). Structural abnormalities in benign childhood epilepsy with centrotemporal spikes (BCECTS). *Seizure*, *27*, 40–46.

Klugah-Brown, B., Luo, C., He, H., Jiang, S., Armah, G. K., Wu, Y., … Yao, D. (2018). Altered dynamic functional network connectivity in frontal lobe epilepsy. *Brain Topography*. https://doi.org/10.1007/s10548-018-0678-z

Li, R., Ji, G. J., Yu, Y., Yu, Y., Ding, M. P., Tang, Y. L., … Liao, W. (2017). Epileptic discharge related functional connectivity within and between networks in benign epilepsy with centrotemporal spikes. *International Journal of Neural Systems*, *27*, 1750018.

Lorio, S., Fresard, S., Adaszewski, S., Kherif, F., Chowdhury, R., Frackowiak, R. S., … Draganski, B. (2016). New tissue priors for improved automated classification of subcortical brain structures on MRI. *NeuroImage*, *130*, 157–166.

Luo, C., Yang, F., Deng, J., Zhang, Y., Hou, C., Huang, Y., … Yao, D. (2016). Altered functional and effective connectivity in anticorrelated intrinsic networks in children with benign childhood epilepsy with centrotemporal spikes. *Medicine (Baltimore)*, *95*, e3831.

Luo, C., Zhang, Y., Cao, W., Huang, Y., Yang, F., Wang, J., … Yao, D. (2015). Altered structural and functional feature of striato-cortical circuit in benign epilepsy with centrotemporal spikes. *International Journal of Neural Systems*, *25*, 1550027.

Martino, M., Magioncalda, P., Huang, Z., Conio, B., Piaggio, N., Duncan, N. W., … Northoff, G. (2016). Contrasting variability patterns

in the default mode and sensorimotor networks balance in bipolar depression and mania. *Proceedings of the National Academy of Sciences of the United States of America*, *113*, 4824–4829.

Marussich, L., Lu, K. H., Wen, H., & Liu, Z. (2017). Mapping white-matter functional organization at rest and during naturalistic visual perception. *NeuroImage*, *146*, 1128–1141.

Palva, J. M., & Palva, S. (2012). Infra-slow fluctuations in electrophysiological recordings, blood-oxygenation-level-dependent signals, and psychophysical time series. *NeuroImage*, *62*, 2201–2211.

Peer, M., Nitzan, M., Bick, A. S., Levin, N., & Arzyt, S. (2017). Evidence for functional networks within the human Brain's white matter. *Journal of Neuroscience*, *37*, 6394–6407.

Pessoa, L. (2014). Understanding brain networks and brain organization. *Physics of Life Reviews*, *11*, 400–435.

Siegel, M., Donner, T. H., & Engel, A. K. (2012). Spectral fingerprints of large-scale neuronal interactions. *Nature Reviews. Neuroscience*, *13*, 121–134.

Smith, S. M., Vidaurre, D., Beckmann, C. F., Glasser, M. F., Jenkinson, M., Miller, K. L., … Van Essen, D. C. (2013). Functional connectomics from resting-state fMRI. *Trends in Cognitive Sciences*, *17*, 666–682.

Wang, X., Zhang, Y., Long, Z., Zheng, J., Zhang, Y., Han, S., … Chen, H. (2017). Frequency-specific alteration of functional connectivity density in antipsychotic-naive adolescents with early-onset schizophrenia. *Journal of Psychiatric Research*, *95*, 68–75.

Wang, Y., Zhu, L., Zou, Q., Cui, Q., Liao, W., Duan, X., … Chen, H. (2018). Frequency dependent hub role of the dorsal and ventral right anterior insula. *NeuroImage*, *165*, 112–117.

Wonderlick, J. S., Ziegler, D. A., Hosseini-Varnamkhasti, P., Locascio, J. J., Bakkour, A., van der Kouwe, A., … Dickerson, B. C. (2009). Reliability of MRI-derived cortical and subcortical morphometric measures: Effects of pulse sequence, voxel geometry, and parallel imaging. *NeuroImage*, *44*, 1324–1333.

Xue, K., Luo, C., Zhang, D., Yang, T., Li, J., Gong, D., … Yao, D. (2014). Diffusion tensor tractography reveals disrupted structural connectivity in childhood absence epilepsy. *Epilepsy Research*, *108*, 125–138.

Yang, T., Guo, Z., Luo, C., Li, Q., Yan, B., Liu, L., … Zhou, D. (2012). White matter impairment in the basal ganglia-thalamocortical circuit of drug-naive childhood absence epilepsy. *Epilepsy Research*, *99*, 267–273.

Yang, T., Luo, C., Li, Q., Guo, Z., Liu, L., Gong, Q., … Zhou, D. (2013). Altered resting-state connectivity during interictal generalized spike-wave discharges in drug-naive childhood absence epilepsy. *Human Brain Mapping*, *34*, 1761–1767.

Yu, R., Chien, Y. L., Wang, H. L., Liu, C. M., Liu, C. C., Hwang, T. J., … Tseng, W. Y. (2014). Frequency-specific alternations in the amplitude of low-frequency fluctuations in schizophrenia. *Human Brain Mapping*, *35*, 627–637.

Zeng, H., Ramos, C. G., Nair, V. A., Hu, Y., Liao, J., La, C., … Prabhakaran, V. (2015). Regional homogeneity (ReHo) changes in new onset versus chronic benign epilepsy of childhood with centro-temporal spikes (BECTS): A resting state fMRI study. *Epilepsy Research*, *116*, 79–85.

Zhang, H., Chen, X., Shi, F., Li, G., Kim, M., Giannakopoulos, P., … Shen, D. (2016). Topographical information-based high-order functional connectivity and its application in abnormality detection for mild cognitive impairment. *Journal of Alzheimer's Disease*, *54*, 1095–1112.

Zhang, Z., Liao, W., Chen, H., Mantini, D., Ding, J. R., Xu, Q., … Lu, G. (2011). Altered functional-structural coupling of large-scale brain networks in idiopathic generalized epilepsy. *Brain*, *134*, 2912–2928.

Zhao, F., Zhang, H., Rekik, I., An, Z., & Shen, D. (2018). Diagnosis of autism spectrum disorders using multi-level high-order functional networks derived from resting-state functional MRI. *Frontiers in Human Neuroscience*, *12*, 184.

Zhao, Z., Tang, C., Yin, D., Wu, J., Gong, J., Sun, L., … Fan, M. (2018). Frequency-specific alterations of regional homogeneity in subcortical stroke patients with different outcomes in hand function. *Human Brain Mapping*, *39*, 4373–4384.

Zhong, C. Q., Liu, R., Luo, C., Jiang, S. S., Dong, L., Peng, R., … Wang, P. (2018). Altered structural and functional connectivity of juvenile myoclonic epilepsy: An fMRI study. *Neural Plasticity*. https://doi.org/10.1155/2018/7392187

Zhou, F., Huang, S., Zhuang, Y., Gao, L., & Gong, H. (2017). Frequency-dependent changes in local intrinsic oscillations in chronic primary insomnia: A study of the amplitude of low-frequency fluctuations in the resting state. *Neuroimage Clinical*, *15*, 458–465.

Zhu, X., He, Z., Luo, C., Qiu, X., He, S., Peng, A., … Chen, L. (2018). Altered spontaneous brain activity in MRI-negative refractory temporal lobe epilepsy patients with major depressive disorder: A resting-state fMRI study. *Journal of the Neurological Sciences*, *386*, 29–35.

Zuo, X. N., Di Martino, A., Kelly, C., Shehzad, Z. E., Gee, D. G., Klein, D. F., … Milham, M. P. (2010). The oscillating brain: Complex and reliable. *NeuroImage*, *49*, 1432–1445.

How to cite this article: Jiang Y, Song L, Li X, et al. Dysfunctional white-matter networks in medicated and unmedicated benign epilepsy with centrotemporal spikes. *Hum Brain Mapp*. 2019;40:3113–3124. https://doi.org/10.1002/hbm.24584